

# CNN vs ELM for Image-Based Malware Classification

Mugdha Jain\* William Andreopoulos\* Mark Stamp\*<sup>†</sup>

## Abstract

Research in the field of malware classification often relies on machine learning models that are trained on high-level features, such as opcodes, function calls, and control flow graphs. Extracting such features is costly, since disassembly or code execution is generally required. In this paper, we conduct experiments to train and evaluate machine learning models for malware classification, based on features that can be obtained without disassembly or execution of code. Specifically, we visualize malware samples as images and employ image analysis techniques. In this context, we focus on two machine learning models, namely, Convolutional Neural Networks (CNN) and Extreme Learning Machines (ELM). Surprisingly, we find that ELMs can achieve accuracies on par with CNNs, yet ELM training requires less than 2% of the time needed to train a comparable CNN.

## 1 Introduction

Malware is software that is designed to disrupt or damage computer systems. According to Symantec, more than 669 million new malware variants were detected in 2017, which was an increase of more than 80% from 2016 [24]. Clearly, malware detection is a critical task in computer security.

Commonly used malware detection techniques can be broadly categorized into anomaly-based and signature-based. However, these strategies have some potential disadvantages. Obfuscation can be used to evade signature-based detection [26], while anomaly-based detection is costly and often yields an unacceptably high false positive rate [15]. Malware detection based on machine learning models may overcome these weaknesses.

Successful machine learning based malware detection approaches have been trained on high-level features such as opcode sequences, function calls, or control flow graphs [7, 10, 18]. However, extracting such high-level features can be costly; hence approaches that do not require extensive pre-processing are preferred, provided that sufficient accuracy can be attained. Specifically, we prefer features that can be obtained without disassembly or code execution.

---

\*Department of Computer Science, San Jose State University

<sup>†</sup>mark.stamp@sjsu.edu

In this research, we consider the Maling dataset [16], which consists of malware samples that have been visualized as images. To obtain these malware images, bytes from executable files are trivially mapped to pixels to create grayscale images [16]. The primary focus of our research is to compare the classification performance of convolutional neural networks (CNN) and extreme learning machines (ELM) for these malware images.

CNNs have been shown to perform well in image classification tasks [17]. In comparison, ELMs are a somewhat less well-known technique, particularly in the field of malware analysis. ELMs are somewhat controversial, but experimental studies have shown that they can produce acceptable predictive performance in some tasks, and at a much lower training cost, as compared to networks that are trained by backpropagation [11]. This makes ELMs attractive for malware classification, particularly when considering the large volume of new malware variants.

When testing CNN and ELM models on the Maling dataset [16], we perform extensive parameter tuning to optimize the performance of each model. For ELMs we also consider an ensemble approach, as previous work has shown that such ensembles can overcome some of the instability issues that are inherent in ELMs [2].

The remainder of this paper is organized as follows. Section 2 discusses relevant previous work. In Section 3 we provide a summary of the dataset used in this research, and we briefly discuss the machine learning techniques that are used. In Section 4, we present and analyze the results of our experiments. Finally, in Section 6, we summarize our results and consider possible avenues for future work.

## 2 Background

Due to the large volume of new malware, antivirus developers must constantly upgrade their methods and algorithms. This makes accurate and rapid detection of malware a critical topic in information security [10].

Malware classification can be based on static or dynamic features, or some combination thereof. Static features are those that are extracted from static files, while dynamic features are extracted during code execution or emulation. Static approaches often use features such as calls to external libraries, strings, and byte sequences for classification [14]. Other static approaches extract higher-level information from binaries, such as sequences of API calls [3] or opcode information [25]. Examples of dynamic features include resource usage and the frequency of calls to specific kernel functions.

A considerable amount of previous work has been done on malware classification. In this section, we discuss a few representative samples of malware classification techniques that have appeared in literature.

## 2.1 Previous Work

Machine learning models for malware detection and classification are trained on features or attributes extracted from executable files. As previously mentioned, examples of such features include opcodes, API calls, control flow graphs, and many others. In many cases the extraction of these features can be costly, so approaches using raw bytes are preferred, if comparable accuracy can be obtained. For example, byte  $n$ -grams have been successfully used as features. As another example, it is possible to treat executable files as images, and apply image analysis techniques.

An opcode-based approach for malware classification is presented in [18]. The opcodes are obtained by disassembling the corresponding `exe` files. The authors then use a technique for determining the relevance of an opcode that is similar to the well-known `tf-idf` (Term Frequency-Inverse Document Frequency) formula, which is a numerical statistic often used in text mining and search engines. In this context, opcode  $n$ -grams are considered as the “words.” These authors also define a Weighted Term Frequency (WTF) to measure of the relevance of each opcode. Although they obtain satisfactory results, their method has a number of disadvantages, including the costly step of disassembling executable files to extract opcodes.

Another opcode-based malware detection technique is proposed in [10]. This work relies on an adjacency matrix based on pairs of consecutive opcodes. The feature vector for each file is constructed by applying the “power iteration” method to the opcode graph. They obtain reasonable results using this technique for the problem of distinguishing malware from benign. However, the authors observe that the power iteration method generally takes a significant amount of time to converge to the dominant eigenvector.

In [20], the authors divide each executable into non-overlapping byte substrings and the frequency histogram of these substrings comprise the feature vectors. They developed a data-mining method that is tested on parts of the file, such as the header or text (code) section. The authors claim that their technique improves detection rates for new malware, as compared to traditional signature-based methods.

The method in [14] is also based on byte  $n$ -grams. In this case, each  $n$ -gram is considered as a boolean attribute, which is `true` if the  $n$ -gram is present in an executable file and `false` otherwise. The top 500  $n$ -grams are selected based on Information Gain (IG). The authors test a variety of machine learning algorithms on these features (SVM, Naïve Bayes, and Decision Tree) and obtain good results for detecting unknown malware instances.

The method proposed in [19] relies on  $n$ -grams as file signatures. The authors employ the  $k$ -nearest neighbor algorithm and experiment with different values of  $n$  for the  $n$ -grams. They achieve their best results using 4-grams.

In [6], the authors propose a technique based on converting executable files to audio. Specifically, they convert each byte of an executable into its corresponding decimal value, which in turn represents a specific musical note in the MIDI encoding scheme. Using this technique, each executable is converted into a MIDI file. The

MIDI file is then converted into an audio signal, and Music Information Retrieval (MIR) techniques are used to extract audio features. Their method achieves an accuracy in excess of 90% for distinguishing malware from benign, based on  $k$ -nearest neighbor, AdaBoost, and Random Forest classifiers.

Extreme Learning Machines (ELM) have been applied to malware detection on the Android platform in [28]. In this work, ELMs are trained on static features, and the results are reasonably strong. In [21], the authors consider the effectiveness of High Performance Extreme Learning Machine (HP-ELM) by varying the features and activation functions of the HP-ELM. Their experiments yield a maximum accuracy of 95.92%.

A two layer ELM is applied to the malware detection problem in [13]. A partially connected network is used between the input and the first hidden layer. This layer is then aggregated with a fully connected network in the second layer. The authors utilize an ensemble to improve the accuracy and robustness of the system.

In [16], the authors propose a method to directly map bytes from an executable file to pixels to create a grayscale image. From the resulting images, they observe that malware files belonging to the same family appear similar in layout and texture. They achieve a classification accuracy of 98% using  $k$ -nearest neighbor. The features considered are based on so-called GIST descriptors, which summarize gradient information in an image. One clear advantage of this method is that neither disassembly nor code execution is required to obtain the features.

The research we present in this paper was motivated to some extent by image-based analysis in [16], as well as the ELM-based thread in [13, 21, 28]. In this paper, we focus on the relative advantages and disadvantages of Convolutional Neural Networks (CNN) and Extreme Learning Machines (ELM) when trained directly on pixel data, rather than, say, high-level GIST descriptors. The features we consider are trivial to extract. In addition, the ELM technique is extremely efficient to train, and we obtain surprisingly strong results, as compared to CNNs.

Next, we provide details on relevant implementation and background topics. Then in Section 4 we present and discuss our experimental results.

## 3 Implementation

In this section, we give a summary of the malware families and the dataset used in this research. Also, we briefly discuss the machine learning techniques that we use in our experiments.

### 3.1 Dataset

We consider malware classification based on the Maling dataset [16]. This dataset contains in excess of 9300 grayscale images belonging to 25 different malware families. This dataset has been used as the basis for several previous research papers, including [27] and the aforementioned [13, 16, 21, 28], among others.

Table 1 lists the 25 families in the Maling dataset and the number of samples that belong to each family. Note that the Maling dataset is extremely imbalanced. For example, the largest family, `Allapple.A`, has nearly one-third of all of the samples and it is more than 36 times as large as the least numerous family, `Skintrim.N`, while the two largest families comprise nearly half of the entire dataset. This imbalance creates some issues when attempting to classifying the samples. We return to this imbalance issue in Section 4.2.5.

Table 1: Type of each malware family

Family	Samples	Family	Samples
<code>Adialer.C</code>	125	<code>Lolyda.AA2</code>	184
<code>Agent.FYI</code>	116	<code>Lolyda.AA3</code>	123
<code>Allapple.L</code>	1591	<code>Lolyda.AT</code>	159
<code>Allapple.A</code>	2949	<code>Malex.gen!J</code>	136
<code>Alueron.gen!J</code>	198	<code>Obfuscator.AD</code>	142
<code>Autorun.K</code>	106	<code>Rbot!gen</code>	158
<code>C2Lop.P</code>	146	<code>Skintrim.N</code>	80
<code>C2Lop.gen!G</code>	200	<code>Swizzor.gen!E</code>	128
<code>Dialplatform.B</code>	177	<code>Swizzor.gen!I</code>	132
<code>Dontovo.A</code>	162	<code>VB.AT</code>	408
<code>Fakerean</code>	381	<code>Wintrim.BX</code>	97
<code>Instantaccess</code>	431	<code>Yuner.A</code>	800
<code>Lolyda.AA1</code>	213	Total	9342

### 3.1.1 Visualization of Malware Files

In [16], the authors describe the technique used to convert malware executables into grayscale images. A given malware binary is read as a vector of 8 bit unsigned integers and then organized into a 2-dimensional array. This is visualized as a grayscale image where each pixel is in the range 0 to 255, where 0 is black and 255 is white. The width of the image is fixed and the height is allowed to vary depending on the file size, as summarized in Table 2.

Figures 1 through 3 show show three different samples from each of three malware families. Specifically, Figure 1 has samples from the `Adialer.C` family, while Figure 2 shows samples of `Dialplatform.B` family, and Figure 3 contains samples of the `Dontovo.A` family. These images indicate that there is considerable intra-family similarity and inter-family differences, at least with respect to these three specific malware families. Intuitively, we would expect image-based analysis to perform well on such data.

Table 2: Image dimensions based on malware size

File Size	Width (pixels)
less than 10kB	32
10kB – 30kB	64
30kB – 60kB	128
60kB – 100kB	256
100kB – 200kB	384
200kB – 500kB	512
500kB – 1000kB	768
greater than 1000kB	1024

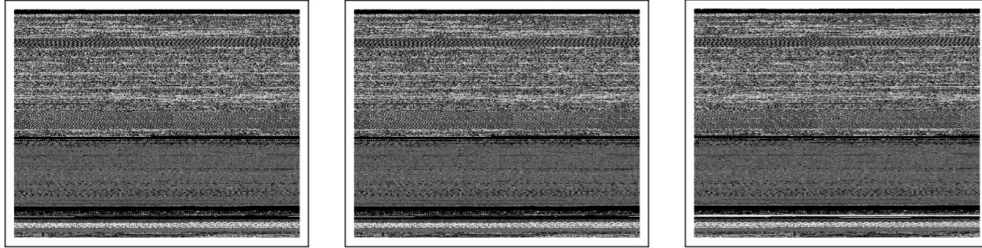


Figure 1: Adialer.C samples

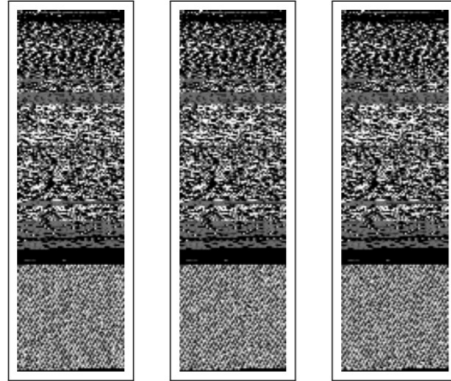


Figure 2: Dialplatform.B samples

### 3.2 Classification Techniques

In this section, we describe the machine learning models considered in this paper. First, we discuss Convolutional Neural Networks and then we outline the main concepts behind Extreme Learning Machines.

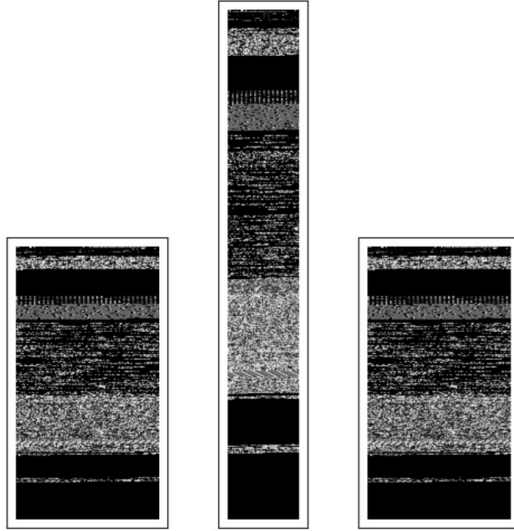


Figure 3: Dontovo.A samples

### 3.2.1 Convolutional Neural Networks

Convolutional Neural Networks (CNN) draw inspiration from the workings and hierarchical structure of the primary visual pathway of the brain. In the 1950s and 1960s, experiments were conducted to understand how the brain perceives the world visually [12]. It was discovered that there are two basic types of visual neuron cells, namely, simple cells (S cells) and complex cells (C cells). These cells activate when they identify basic shapes such as lines in a fixed area and at a specific angle.

A CNN is a type of feed-forward neural network for processing data that takes a 2-dimensional or higher-dimensional matrix as input. CNNs have proven highly effective for image analysis. CNNs typically include multiple convolutional layers, one or more pooling layers, and a fully-connected output layer. All of the CNN experimental results discussed in this paper are based on models trained using Keras [4].

Convolutional layers are the main building blocks of CNNs. A discrete convolution is a sequence that is itself a composition of two sequence—more precisely, a discrete convolution is computed as a sum of pointwise products. Let  $c = x * y$  denote the convolution of sequences  $x = (x_0, x_1, x_2, \dots)$  and  $y = (y_0, y_1, y_2, \dots)$ . Then  $c_k$ , the  $k^{\text{th}}$  element of the convolution, is given by

$$c_k = \sum_{k=i+j} x_i y_j = \sum_i x_i y_{k-i}$$

We can view this process as  $x$  acting as a “filter” (or kernel) on the sequence  $y$  over a sliding window. The concept of a discrete convolution is easily extended to higher-dimensional data. With CNNs, we generally treat color images as 3-dimensional

arrays, with the third dimension given by the red, green, and blue color planes of the RGB encoding.

In a CNN, the coefficients of the convolutions (i.e., weights) are learned via training, with this training typically completed via the backpropagation algorithm. Convolutions serve to greatly reduce the number of weights, as compared to a fully connected network, and thus make training on images practical. In addition, when applying CNNs to images, we obtain a high degree of translation invariance, which is highly desirable in image analysis, and serves to greatly reduce the overfitting that would otherwise tend to occur.

The first convolutional layer of a CNN is applied to the input image. This is illustrated in Figure 4, where the input consists of an RGB image, which is treated as 3-dimensional data. In this case, five filters are learned at the first layer—by randomly initializing the weights of the filters, the CNN can learn multiple filters at each layer. Thus, the next convolutional layer can also be applied to higher-dimensional data.

After the first convolutional layer, subsequent convolutional layers are applied to the output of previous convolutional layers. Hence, we compute convolutions of convolutions. At the first convolutional layer, the filters learn intuitive features, such as edges and basic shapes, whereas the second convolutional layer learns more abstract features, such as “texture.” Convolutional layers learn progressively more abstract features that ultimately can be used to distinguish, say, a picture of a cat from that of a dog.

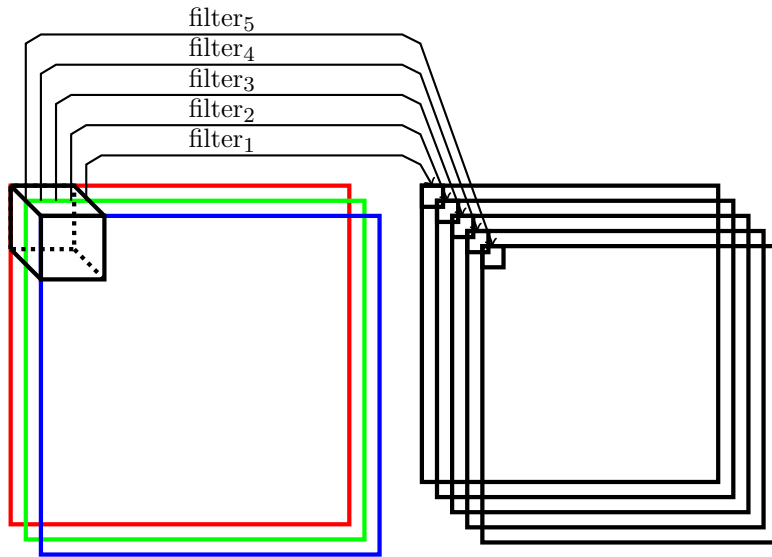


Figure 4: First convolutional layer with stack of 5 filters (RGB image)

Between each pair of convolutional layers, it is common to add a pooling layer. The function of pooling is to reduce the dimensionality, and thus reduce the training



time. Pooling might also improve various desirable properties, such as translation invariance. There are several types of pooling functions, with max pooling being the most common. Max pooling consists of simply selecting the maximum value over a given filter block. Figure 5 illustrates max pooling over a 2-dimensional feature vector.

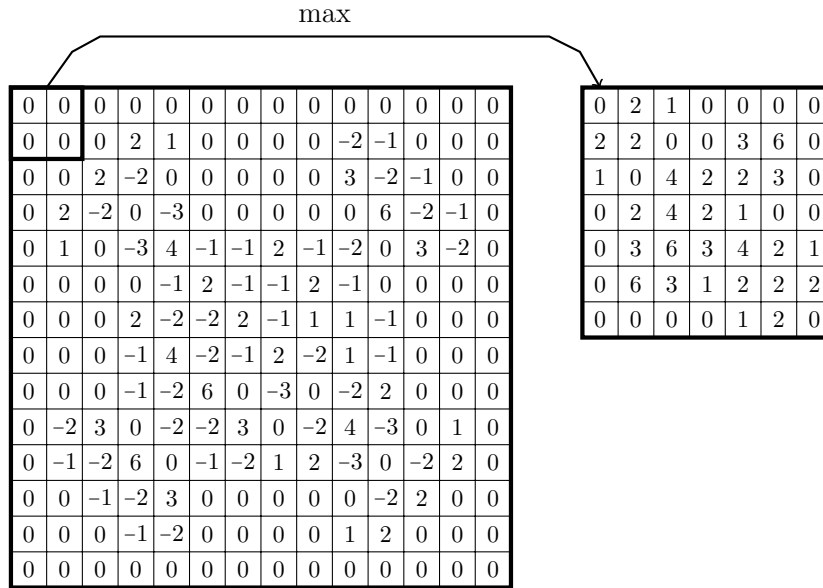


Figure 5: Max pooling layer ( $2 \times 2$ )

Note that convolutional layers typically use a stride of one, while pooling uses a stride equal to the filter width, which serves to further increase the downsampling effect of pooling. Recently, it has become popular to use convolutional layers with a stride greater than one in place of pooling layers.

### 3.2.2 Extreme Learning Machine

As with most aspects of ELMs, the origin of the technique is somewhat controversial. The unfortunate terminology of “Extreme Learning Machine” was apparently first used in [9]. Regardless of the origin of the technique, ELMs are essentially randomized feedforward neural networks that effectively minimize the cost of training.

An ELM consists of a single layer of hidden nodes, where the weights between inputs and hidden nodes are randomly initialized and remain unchanged throughout training. The weights that connect the hidden nodes to the output are trained, but due to the simple structure of an ELM, these weights can be determined by solving linear equations—more precisely, by solving a linear regression problem. Since no backpropagation is required, ELMs are far more efficient to train, as compared to other neural network architectures. However, since the weights in the hidden layer are not optimized, we will typically require more weights in an ELM, which implies

that the testing phase may be somewhat more costly, as compared to a network trained by backpropagation. Nevertheless, in applications where models must be trained frequently, ELMs can be competitive.

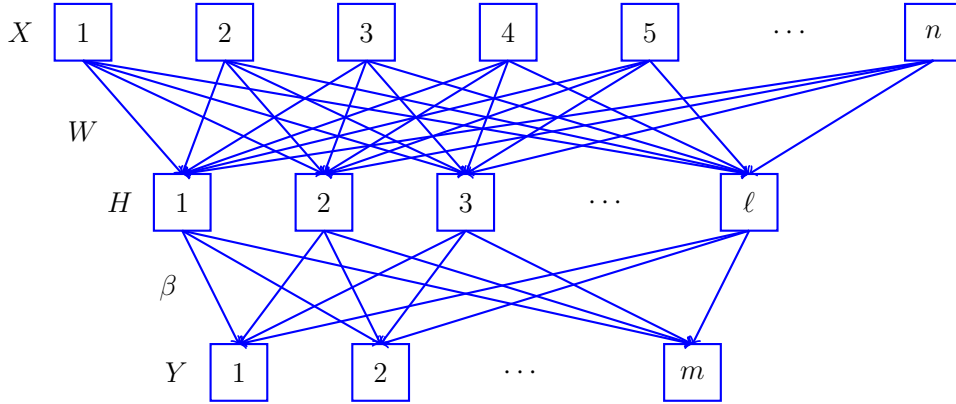


Figure 6: Architecture of an ELM model

Consider the ELM architecture shown in Figure 6, where  $X$  denotes the input layer,  $H$  is the hidden layer and  $Y$  is the output layer. In this example, there are  $N$  samples of the form  $(x_i, y_i)$  for  $i = 1, 2, \dots, N$ , where  $x_i = (x_{i_1} \ x_{i_2} \ \dots \ x_{i_n})^T$  is the feature vector for sample  $i$  and  $y_i = (y_{i_1} \ y_{i_2} \ \dots \ y_{i_m})^T$  are the output labels, where  $T$  indicates the transposition operation. Then the input and output for the ELM are as  $X = (x_1 \ x_2 \ \dots \ x_n)^T$  and  $Y = (y_1 \ y_2 \ \dots \ y_m)^T$ , respectively. In this example, the hidden layer  $H$  has  $\ell$  neurons. We denote the activation function of the hidden layer as  $g(x)$ .

To train an ELM, we randomly selects the weight matrix that connects the input layer  $X$  to the hidden layer  $H$ . We denote this randomly-assigned weight matrix as  $W = (w_1 \ w_2 \ \dots \ w_\ell)$  where each  $w_i$  is a column vector. We also randomly select the bias matrix  $B = (b_1 \ b_2 \ \dots \ b_\ell)$  for this same layer. During the training phase, both  $W$  and  $B$  remain unchanged.

After  $W$  and  $B$  have been initialized, the output of the hidden layer  $H$  is given by

$$H = g(WX + B).$$

The output of the ELM is denoted as  $Y$  and is calculated as

$$Y = H\beta$$

where  $\beta$  is the weight matrix for the output layer.

The values of the weights  $\beta$  at the hidden layer are learned via linear least squares, and can be computed using  $H^\dagger$ , the Moore-Penrose generalized inverse of  $H$ , as discussed below. It is worth emphasizing that the only parameters that are learned in the ELM are the elements of  $\beta$ .

Given that  $Y$  is the desired output, a unique solution of the system based on least squared error can be found as follows. We denote the Moore-Penrose generalization inverse of  $H$  as  $H^\dagger$ , which is defined as

$$H^\dagger = \begin{cases} (H^T H)^{-1} H^T & \text{if } H^T H \text{ is nonsingular} \\ H^T (H H^T)^{-1} & \text{if } H H^T \text{ is nonsingular} \end{cases}$$

Then the desired solution  $\beta$  is give by

$$\beta = H^\dagger Y$$

After calculating  $\beta$ , the training phase ends. For each test sample  $x$ , the output  $Y$  can be calculated as

$$Y = g(C(x))\beta$$

where  $C(x)$  is defined below. The entire training process is extremely efficient, particularly in comparison to the backpropagation technique that is typically used to train neural networks [23].

For the research reported in this paper, we use the Python implementation of ELMs given in [5]. This implementation uses input activations that are a weighted combination of two functions that are referred to as an ‘‘MLP’’ kernel and an ‘‘RBF’’ kernel—we employ the same terminology here. The MLP kernel is simply the linear operation

$$M(x) = Wx + B$$

where the weights  $W$  and biases  $B$  are randomly selected from a normal distribution. This is the kernel function that is typically associated with a standard ELM.

The RBF kernel is considerably more complex, and is based on generalized radial basis functions as defined in [8]. The details of this RBF kernel go beyond the scope of this paper; see [8] for additional information and, in particular, examples where this kernel is applied to train ELMs. We use the notation  $R(x)$  to represent the RBF kernel. Also, it is worth noting that the RBF kernel is much more costly to compute, and hence its use does somewhat negate one of the major advantages of an ELM. We provide timing comparisons for these kernels in Section 4.

The input activations are given by

$$C(x) = \alpha M(x) + (1 - \alpha)R(x) \tag{1}$$

where  $0 \leq \alpha \leq 1$  is a user-specified mixing parameter. Note that for  $\alpha = 0$  we use only the MLP kernel  $M(x)$  and for  $\alpha = 1$ , only the RBF kernel  $R(x)$  is used.

## 4 Experiments and Results

In this section, we discuss the results of malware classification experiments involving the Maling dataset. First we consider our CNN experiments, then we discuss our ELM results. Finally, we compare the results obtained using these two approaches.

## 4.1 CNN Experiments

For the experiments discussed in this section, each CNN model was trained for 50 epochs with the `relu` activation function. Various CNN architectures with different combinations of convolution, pooling, and dense (fully-connected) layers are considered. We also give results related to tuning of the hyperparameter, including input image size, batch size, number of filters, filter size, and pooling size.

### 4.1.1 One Convolutional Layer

Our one-convolutional layer models were trained on different input image sizes ( $32 \times 32$ ,  $64 \times 64$ , and  $128 \times 128$  pixels) and different number of filters (32 and 64). Each of these CNN models uses  $3 \times 3$  filters, a fully connected layer with 128 neurons, and an output layer with 25 neurons corresponding to the classes in the Maling dataset. A `softmax` activation function is used in each case. Table 3 summarizes our results for these six cases. We see that the larger image size of  $128 \times 128$  clearly outperforms the smaller image sizes.

Table 3: CNN models with one convolutional layer

Image Size	Filters	Accuracy
$32 \times 32$	32	0.8400
$32 \times 32$	64	0.8467
$64 \times 64$	32	0.9340
$64 \times 64$	64	0.9245
$128 \times 128$	32	<b>0.9630</b>
$128 \times 128$	64	0.9589

Classwise accuracies for the  $128 \times 128$  experiments in Table 3 are summarized in Figure 7. We observe that training these CNNs on images of size  $128 \times 128$  with 32 filters results in an accuracy of 96.3%. The confusion matrix for this best case is given in Figure 8. This model is able to achieve an accuracy of above 90% for 16 out of the 25 classes in the dataset—only one family, namely, `Autorun.K`, has an accuracy below 50%.

The confusion matrix in Figure 8 also shows which specific malware families are frequently misclassified. For example, we see that 5 of the 12 samples of the family `Swizzor.gen!I` are misclassified as belonging to `Swizzor.gen!E`, which is not surprising, given that they are both variants of the Swizzor trojan family. The visual similarity between malware images from these families can be seen in Figure 9.

Another interesting misclassification case occurs for samples of `Autorun.K`, which are all misclassified as belonging to the family `Yuner.A`. The visual similarity between these two families is also quite obvious, as can be seen in Figure 10.

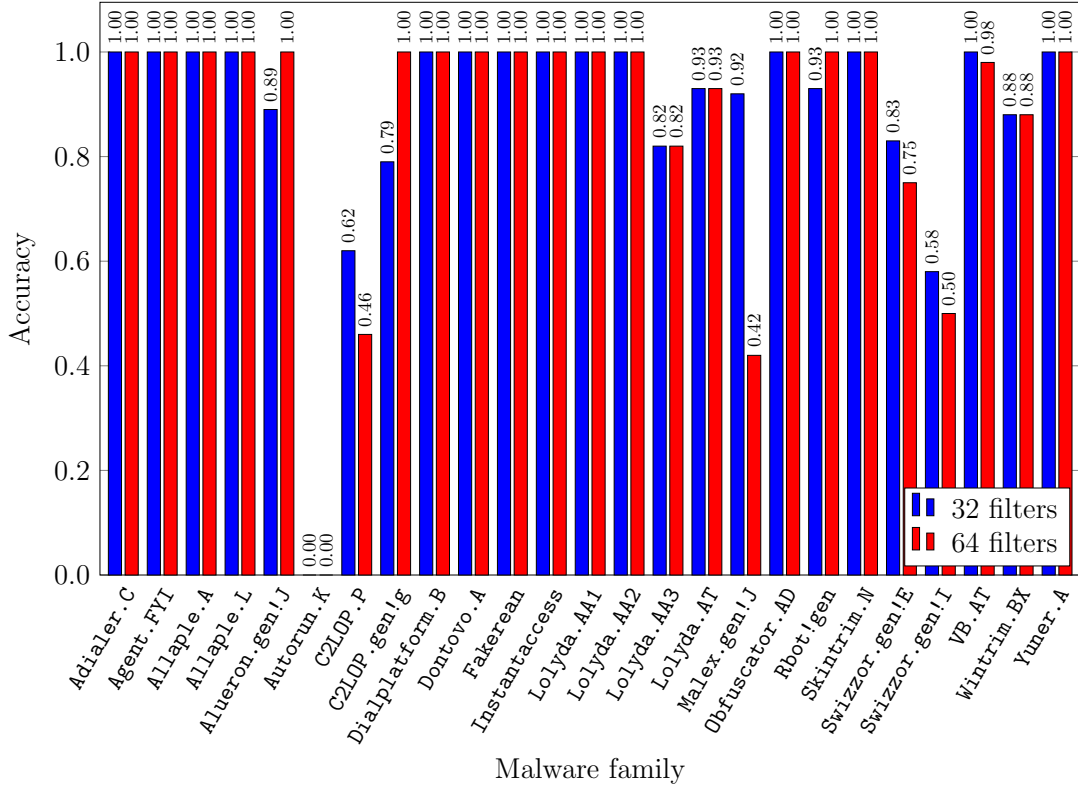


Figure 7: CNN with one convolutional layer ( $128 \times 128$  images)

We note that for all three image sizes considered, increasing the number of filters has minimal effect on the one-convolutional layer CNN accuracy. This could be attributed to the fact that images in the dataset are in grayscale and have relatively simple structure, and hence only a small number of filters is required. In contrast, there is a definite increase in the overall accuracy when the size of the input image is increased. However, there are some anomalies, such as *Autorun.K*, which is predicted with 100% accuracy for all models based on image size  $32 \times 32$ , but for  $64 \times 64$  and  $128 \times 128$  size images, samples of this family are consistently misclassified as *Yuner.A*.

#### 4.1.2 Two Convolutional Layers

This section briefly describes the experiments conducted with CNN models with two convolutional layers. These models were trained for similar cases of image size, filters, pooling layer, etc., as in the previous section. However, since we have two convolutional layers, we experiment with different numbers of filters in these layers. Table 4 summarizes our results for these two convolutional layer models.

The best results in Table 4 were obtained with input images of size  $128 \times 128$

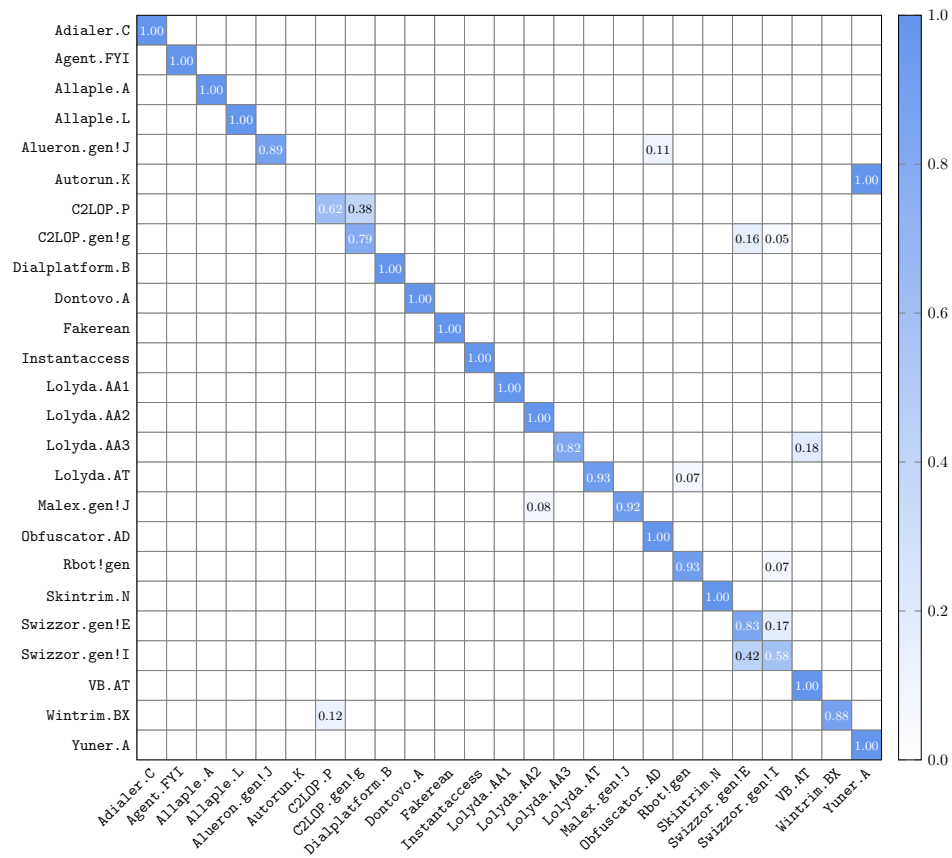
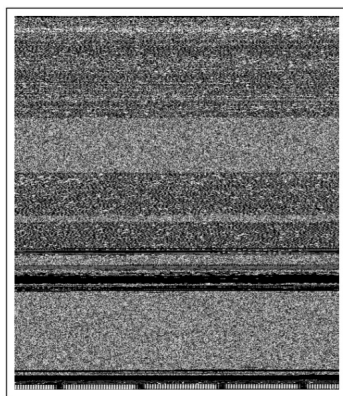
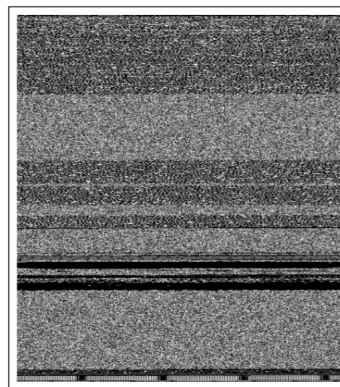


Figure 8: Confusion matrix for best CNN model ( $128 \times 128$  images and 32 filters)

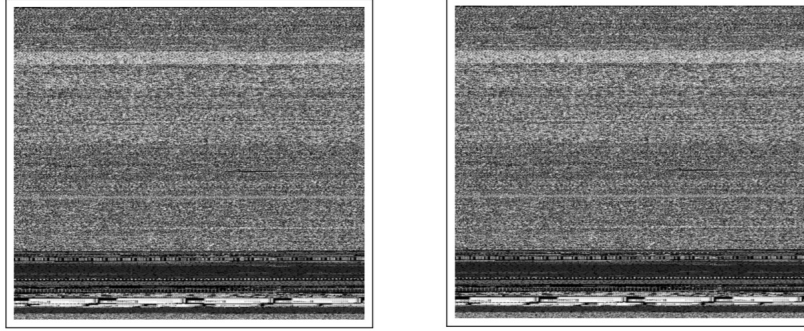


(a) Swizzor.gen!I



(b) Swizzor.gen!E

Figure 9: Samples from Swizzor families



(a) Autorun.K

(b) Yuner.A

Figure 10: Samples from a pair of similar families

Table 4: CNN models with two convolutional layers

Image Size	Number of Filters		Accuracy
	First Layer	Second Layer	
$32 \times 32$	32	32	0.820
$32 \times 32$	32	64	0.816
$32 \times 32$	64	32	0.823
$32 \times 32$	64	64	0.834
$64 \times 64$	32	32	0.934
$64 \times 64$	32	64	0.928
$64 \times 64$	64	32	0.950
$64 \times 64$	64	64	0.943
$128 \times 128$	32	32	0.921
$128 \times 128$	32	64	<b>0.957</b>

pixels with 32 and 64 filter maps. This model achieved an overall accuracy of 95.67%. The classwise accuracies for this case are summarized in Figure 11.

Our best two-convolutional layer model in Table 4 is just slightly below the best one-layer model in Table 3. Since training time is significantly increased for two-layer models, and since a one-convolutional layer model performs best, the one-layer model is the clearly the best among the CNN architectures that we tested.

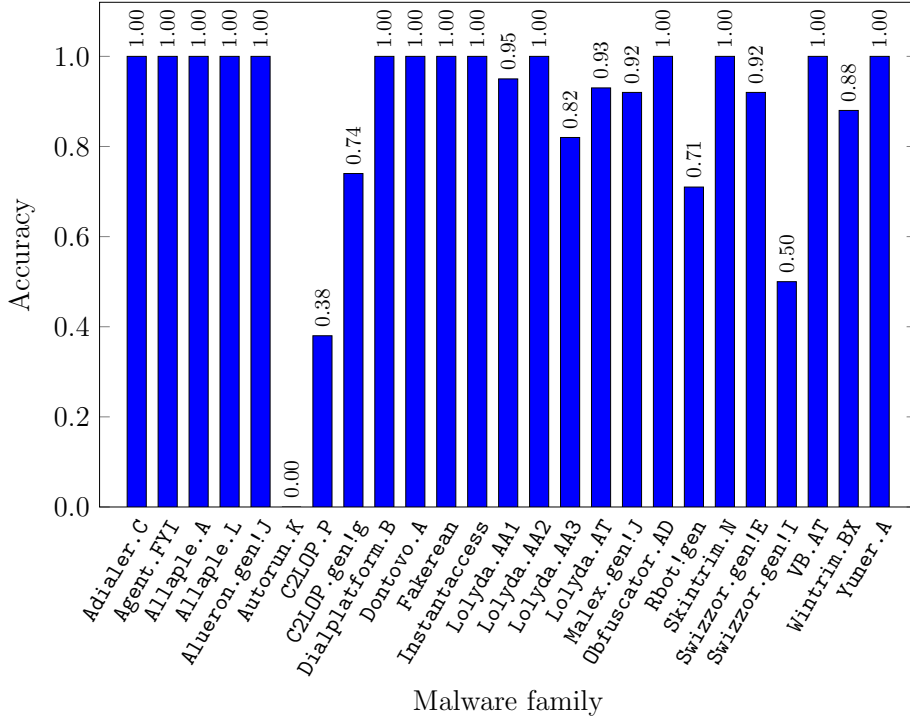


Figure 11: CNN with two convolutional layers,  $128 \times 128$  images, and (32, 64) filters

## 4.2 ELM Experiments

This section describes our ELM experiments and results. Analogous to the CNN experiments discussed in the previous section, we test a wide variety of ELM architectures. For ELMs, the number of parameters are relatively few—we experiment with the number of neurons in the hidden layer and the choice of activation functions. For each combination of parameters, we train and test 50 ELMs, and evaluate the performance in terms of the average accuracy. In addition, also consider ensembles of ELMs, we perform experiments to analyze the stability of our models, and we consider the effect of regularization—in the form of dropouts.

### 4.2.1 Input Activation

In this section, we experiment with the input activation function parameter  $\alpha$ , which appears in equation (1). Recall that the input activation function is a linear combination of a so-called MLP kernel and an RBF kernel, with  $\alpha$  determining the relative weighting of these two kernels.

We trained 50 ELMs on images of size  $64 \times 64$ , with  $\alpha = 1$ . For this choice of the parameter  $\alpha$ , only the highly-efficient MLP kernel is used. We refer to this as pure MLP activation.



At the hidden layer, we experiment with the activation functions `tanh`, `relu`, `softlim`, `hardlim`, `multiquadric`, and with number of neurons selected from

(128, 256, 512, 1024, 2048, 4096).

Figure 12 shows the average accuracies over 50 ELMs with the specified parameters.

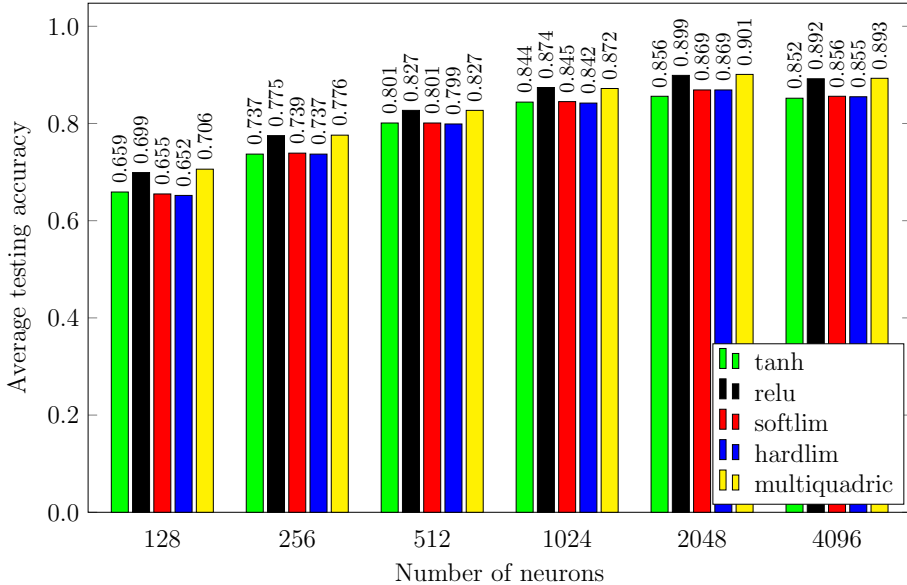


Figure 12: Average accuracy of 50 ELM models ( $\alpha = 1$ )

From the results in Figure 12, it is clear that the `relu` and `multiquadric` activation functions consistently perform somewhat better than `tanh`, `softlim`, and `hardlim`. Moreover, the average accuracies increase with more neurons in the hidden layer, until a slight drop from 2048 to 4096 neurons.

Despite the fact that the weights  $W$  and biases  $B$  are selected at random, the ELMs in these experiments perform surprisingly consistently. The standard deviations in the testing accuracies are given in Table 5, and serve to confirm a high degree of consistency, regardless of the activation function.

In Figure 13 we compare training and testing accuracies as the number of neurons increases. In each of these experiments, we let  $\alpha = 1$  and the results are an average of 50 ELMs. We observe that the training accuracy reaches 1.0 with 4096 neurons, and this holds for all of the activation functions tested. However, in every case, the test (or validation) accuracy declines at 4096 neurons, as compared to 2048 neurons. This is a clear sign of the models overfitting when 4096 neurons are used.

Next, we generate 50 ELMs with the same parameters as above, except that we use  $\alpha = 0.5$  instead of  $\alpha = 1$ . In this case input activation is equally split between the MLP and RBF kernels. Figure 14 shows the average accuracies across these 50 ELM models for the indicated parameters.

Table 5: Standard deviation over 50 ELM models ( $\alpha = 1$ )

Activation	Neurons					
	128	256	512	1024	2048	4096
tanh	0.014	0.013	0.010	0.008	0.096	0.007
relu	0.013	0.011	0.008	0.007	0.007	0.008
softlim	0.016	0.015	0.009	0.009	0.009	0.009
hardlim	0.016	0.011	0.008	0.007	0.008	0.007
multiquadric	0.012	0.011	0.007	0.008	0.005	0.006

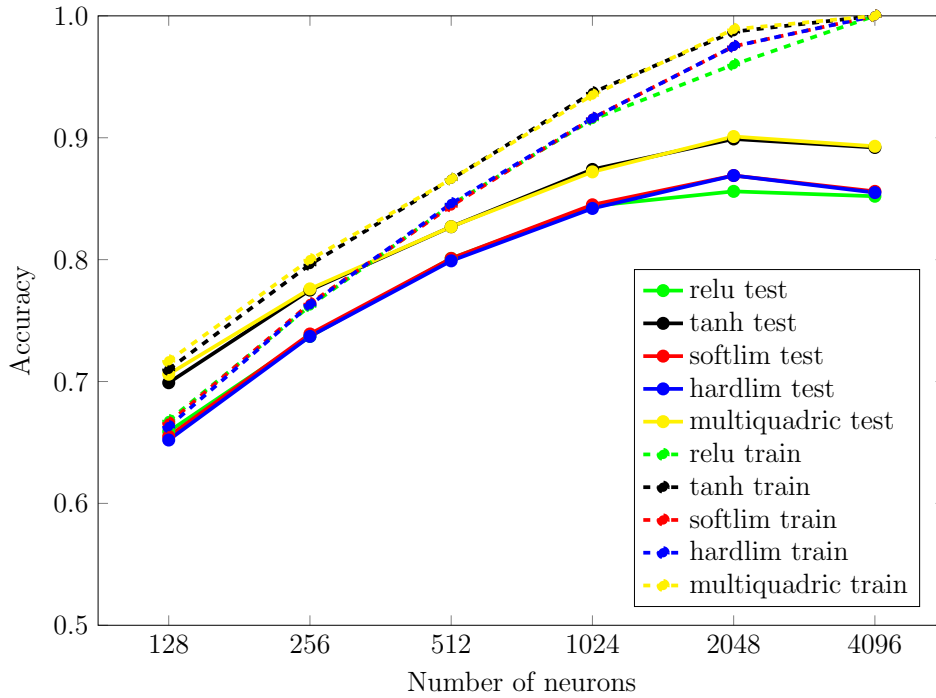


Figure 13: Training/testing accuracy vs number of neurons ( $\alpha = 1$ )

We see that the accuracies for the  $\alpha = 0.5$  case, as summarized in Figure 14, are virtually indistinguishable from the results for the  $\alpha = 1$  case as given in Figure 12. In both cases, the **relu** and **multiquadric** activation functions consistently outperform **tanh**, **softlim**, and **hardlim**.

We also conducted experiments with a pure RBF kernel, i.e.,  $\alpha = 0$ , but the results were no better than the  $\alpha = 0.5$  case. Furthermore, for any  $0 \leq \alpha < 1.0$ , the training time is much greater than for the  $\alpha = 0$  case. This is clearly illustrated in Figure 15, where timings for  $\alpha = 0$  and  $\alpha = 0.5$  are given.

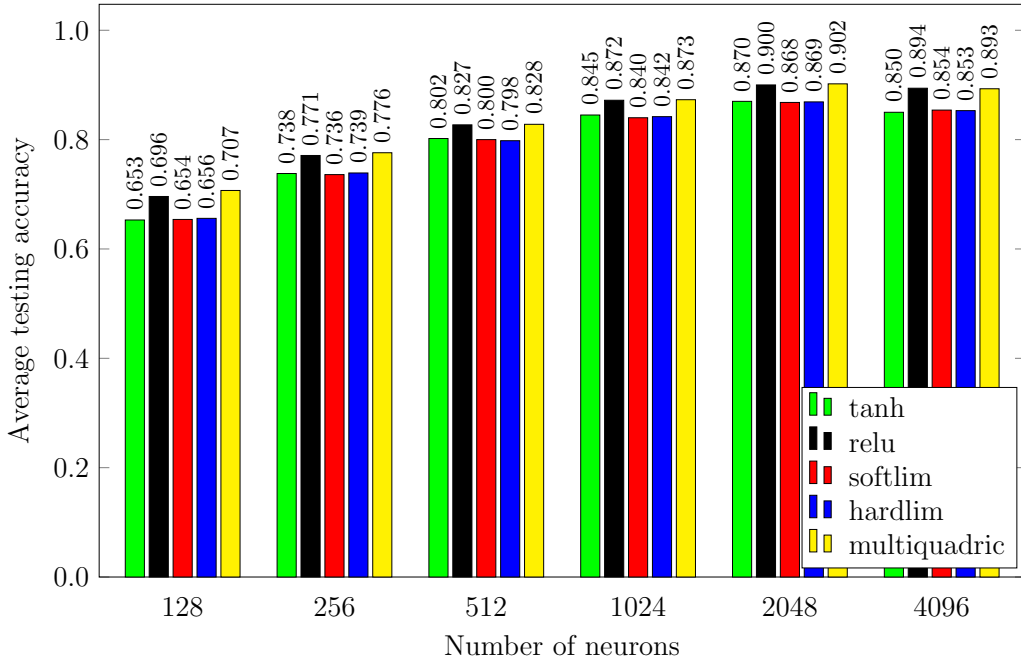


Figure 14: Average accuracy of 50 ELM models ( $\alpha = 0.5$ )

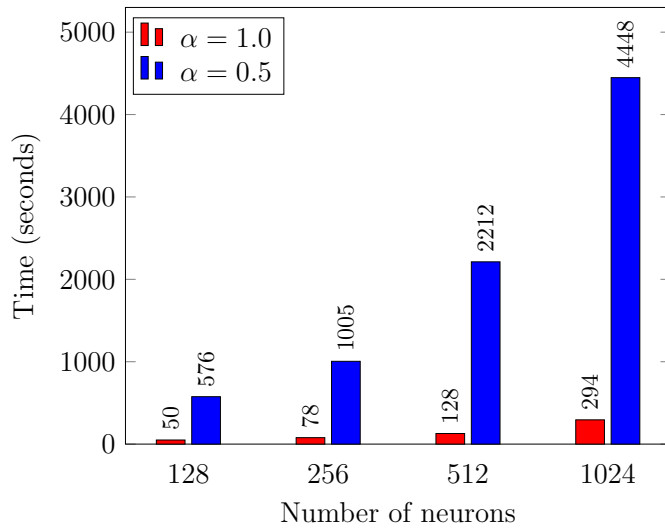


Figure 15: Training time for 50 ELMs

The  $\alpha = 1$  case is the most efficient and it performs as well as the  $\alpha = 0.5$  case. We also find that 1024 neurons performs best, and that the `relu` activation outperforms the other activations. Hence, we have selected the parameters in Table 6 for all ELM experiments discussed below, unless explicitly stated otherwise.

Table 6: ELM parameters

Activation	Mixing	Neurons
relu	$\alpha = 1$	1024

### 4.2.2 Majority Vote Ensembles

Ensemble learning consists of combining several models into one, which can serve to decrease the variance and the bias, thus improving predictions. In this section, we consider an ensemble technique consisting of a majority vote of classifiers. Here, the individual classifiers are 50 ELMs and, again, these are combined by taking a simple majority vote of their decisions. Since we have 25 classes, it is possible that there could be ties in the voting, in which case we would simply make a random selection from among those receiving the most votes. However, we found no case where there was a tie vote in any of our experiments.

Figure 16 shows that with increasing number of neurons, our ensemble accuracy consistently increases. Furthermore, the ensemble classifier always outperforms the average case for the individual ELMs.

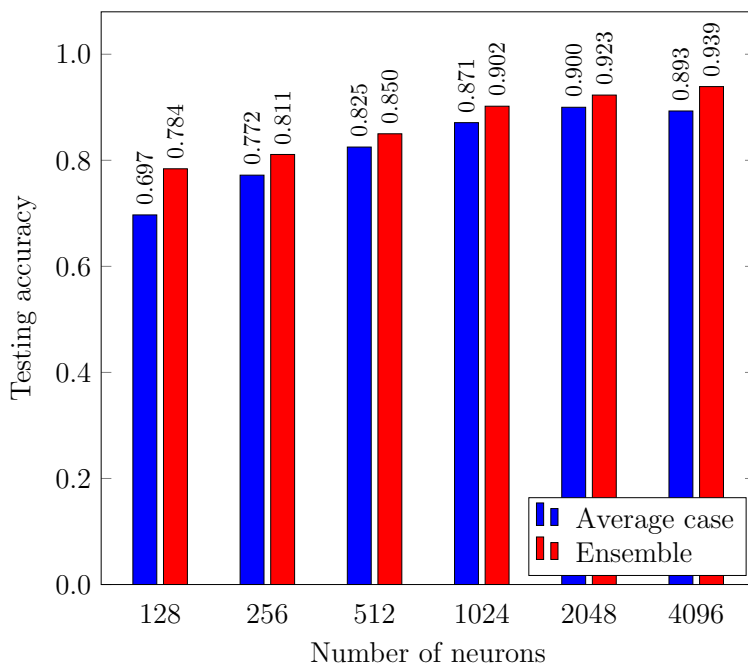


Figure 16: Ensemble classifier accuracy ( $64 \times 64$  images)

### 4.2.3 Dropouts

In a fully connected layer, each neuron is connected to all input nodes. Dropouts are neurons that are ignored during the training phase—an example appears in Figure 17. The neurons to be dropped are chosen at random with a probability  $p$ , with typically only a small percentage of neurons are dropped [22]. Dropouts offer a simple form of regularization, and hence serve to reduce overfitting.

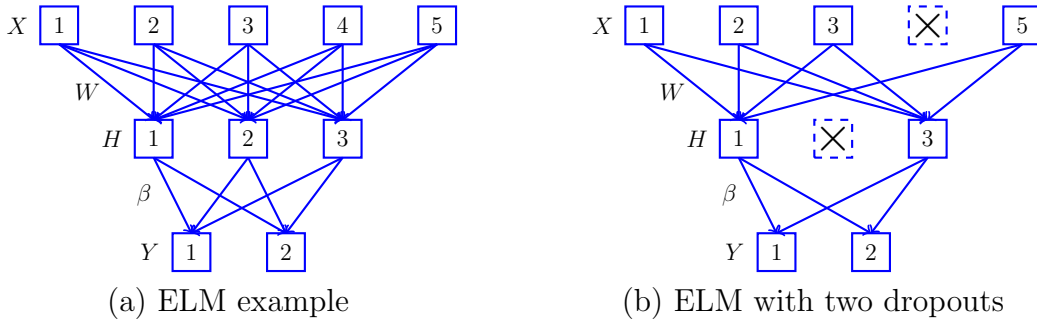


Figure 17: Dropouts

Since ELMs have no backpropagation, we take a slightly different approach to dropouts in our ELM experiments. We implement an algorithm that connects each neuron in the hidden layer to four randomly selected input nodes. This technique results in a relatively large percentage of connections being lost. Such an aggressive approach is needed with ELMs, since training occurs in a single step, as opposed to multiple epochs in backpropagation.

Figure 18 gives our average and ensemble accuracies across 50 ELMs, for both the fully connected and dropout cases. Dropout ELMs consistently perform better than fully connected ELMs. In addition, the corresponding ensemble classifiers consistently outperform the corresponding non-ensemble classifiers.

### 4.2.4 One Dimensional Input

An executable file can be viewed as a sequence of bytes. When executable files are converted to images, sequential patterns present in the executables may be lost, depending on the image dimensions. To preserve these sequential patterns, we consider a different technique for generating ELM input feature vectors. Instead of treating the Maling samples as images, we consider each as a one-dimensional vector by simply reading the pixels from left to right from top to bottom. Since the images in the dataset are of varying dimensions, these one-dimensional vector also differs in length.

We convert all of our one-dimensional vectors to a fixed length  $N$  by simply averaging elements. Specifically, suppose that a vector  $V$  is of length  $T$ . If necessary, we pad  $V$  so that it is evenly divisible by  $N$ . Let  $V'$  be this new vector, and let  $T'$

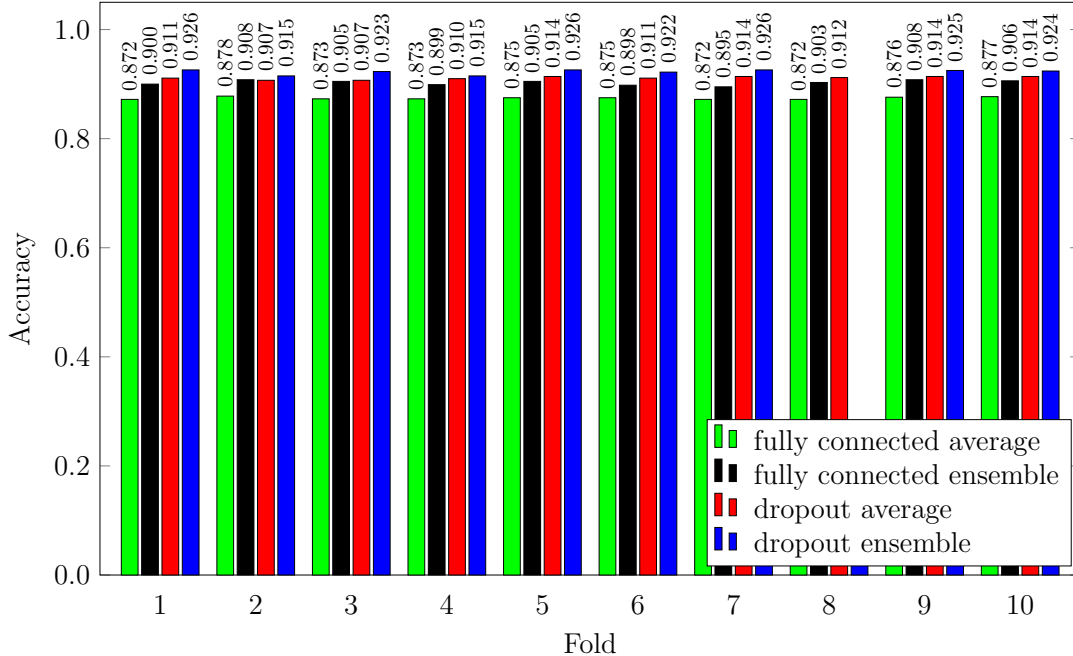


Figure 18: Fully connected vs dropout ELMs ( $64 \times 64$  images)

be its length. Then we generate a vector  $X$  of length  $N$  where

$$x_i = \frac{v'_i + v'_{i+1} + \dots + v'_{i+N-1}}{\ell}$$

where  $\ell = T'/N$ . We refer the resulting  $X$  as an  $N \times 1$  vectors to emphasize that it is 1-dimensional, as opposed to the 2-dimensional image from which it was derived. These  $N \times 1$  vectors serve as the features for all experiments in this section.

Our first one-dimensional input experiment consists of ensemble classifiers comprised of 50 dropout ELMs. The input to each ELM is a vector of dimension  $512 \times 1$ . We train one such ensemble ELM with 512 neurons, another with 1024, and a third with 2048 neurons. In each case, we use  $\alpha = 1$  and `relu` activation functions. Figure 19 (a) shows the average ensemble classifier accuracy, and we see that the best accuracy is achieved for ELMs with 1024 neurons.

We consider an additional set of experiments using 1024 neurons and the same parameters as in our previous experiment, but varying the input vector length. Figure 19 (b) shows increasing the input vector length beyond  $512 \times 1$  has a minimal effect on the accuracy. Interestingly, we see little variability in these one-dimensional input length results. This is in contrast to the CNN results on 2-dimensional images, where the image size was a significant parameter.

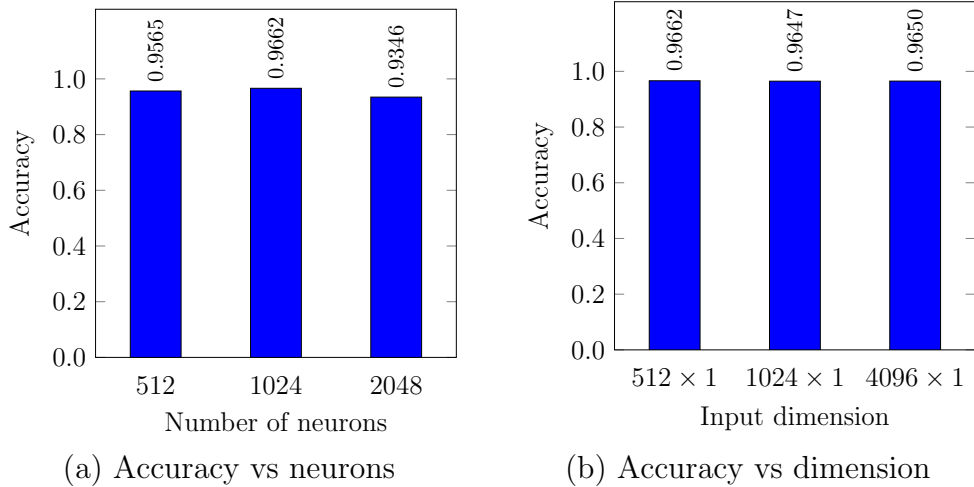


Figure 19: Average ensemble accuracy

#### 4.2.5 Weighted ELMs

The Maling dataset is highly imbalanced, as can be seen from the numbers in Table 1. In a classification task with such unequal number of samples per class, predictions are naturally biased towards the classes with the most data. To better account for imbalanced class distributions, a weighted ELM is proposed in [1], which employs a weighted linear system for the solution of the output layer weights. To compute the necessary weights, we let

$$S_j = \text{total number of samples in class } j$$

and

$$S = \sum S_j$$

where the sum is over all classes in the dataset. Denote row  $j$  of  $H$  as  $h_j$  and row  $j$  of  $Y$  as  $y_j$  and let  $c_j = \sqrt{S/S_j}$ . Then we compute

$$h'_j = c_j h_j \quad \text{and} \quad y'_j = c_j y_j$$

and form the weighted matrices  $H'$  and  $Y'$  from these weighted rows. The weighted ELM is trained as discussed in Section 3.2.2, except that we use  $H'$  and  $Y'$  and place of  $H$  and  $Y$ .

For our weighted ELM experiments, we consider an ensemble of 50 dropout ELMs. The individual ELMs have 1024 neurons, and we use  $\alpha = 1$  with `relu` activation functions, and one-dimensional input vectors of size  $1024 \times 1$ . Figure 20 compares the accuracy of the weighted and unweighted ensemble classifiers. The average accuracy for the unweighted model is 96.5%, while for the weighted model we obtain a slight improvement at 97.7%.

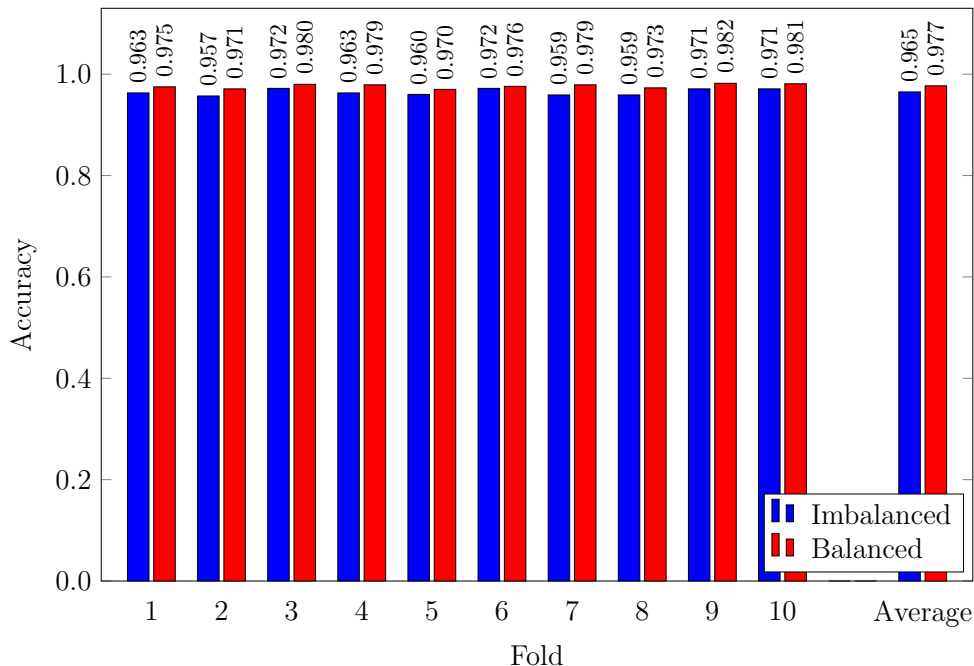


Figure 20: Weighted ELM accuracy ( $1024 \times 1$  input)

## 5 Discussion

Our best CNN model achieves an overall accuracy of 96.3%. This CNN is based on an input image of size  $128 \times 128$ , it uses one convolutional layer with 32 filters, each of size  $3 \times 3$ , a max-pooling layer with a filter of size  $2 \times 2$ , a dense layer of 128 neurons, and 25 neurons in the output layer. In comparison, our best ELM-based model achieves an accuracy of 97.7%. This ELM-based model consists of an ensemble classifier built on 50 ELMs with dropouts, each of which uses a class weighting technique, with  $\alpha = 1$  and 1024 neurons in the hidden layer. These ensembled ELMs all use `relu` activation functions and are trained on one-dimensional input of size  $1024 \times 1$ . Figure 21 gives the classwise F1 score comparison for our best CNN and ELM models.

In addition to outperforming CNNs overall, our ELM achieves equal or better F1 scores on 18 of the 25 classes. It is interesting to note that the ELMs are also able to predict at least some instances of all 25 families, whereas the CNN sometimes misses an entire family. For example, in Figure 21, we see that the CNN misclassifies all instances of the `Autorun.K` family, while in stark contrast, the ELM is able to correctly classify all samples from this particular family.

Finally, we consider the training efficiency of ELMs in comparison to CNNs. In Figure 22 we give timings for some of the architectures discussed above. In each case, the time listed is for training 50 models of the specified type.



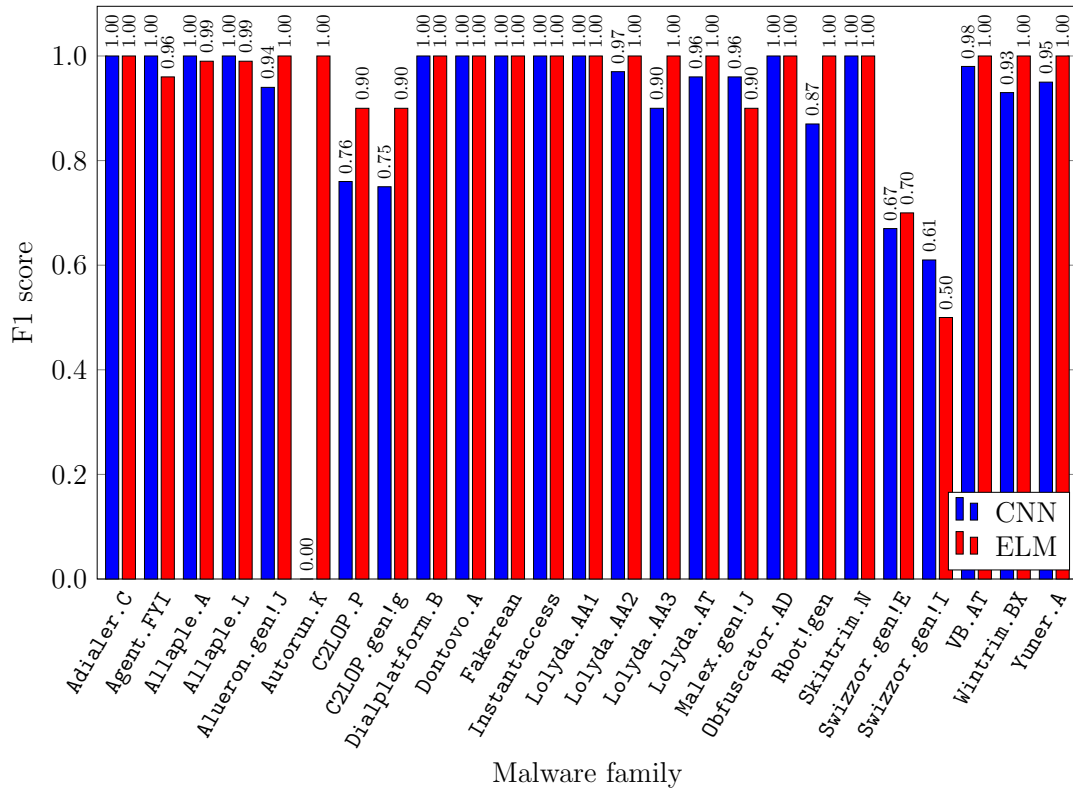


Figure 21: Classwise F1 scores for CNN and ELM

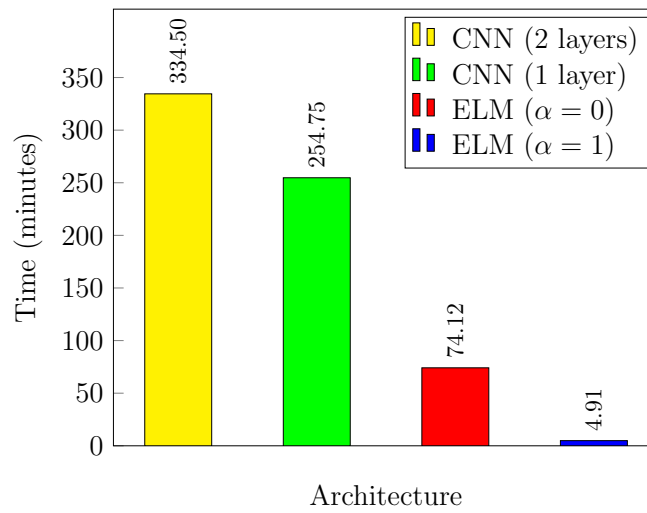


Figure 22: Training time comparison of CNN and ELM

We see that standard ELMs with the MLP kernel (i.e., the  $\alpha = 1.0$  case) can be trained in about 2% of the time required to train a CNN having just a single convolution layer. In comparison to 2-convolutional layers, we can train a standard ELM in less than 1.5% of the time required for the CNN. And, even with the computationally expensive RBF kernel, the ELM can be trained in less than 30% of the time required by the fastest CNN architecture. Given that we obtained our best results with an ELM using the MLP kernel, these results show a clear advantage of ELMs in cases where a large number of models are to be trained.

## 6 Conclusion

In this paper, we have compared CNNs and ELMs for image-based malware classification. We considered a variety of different CNN architectures, varying the input image size, number of convolutional layers, and number of filters. In another set of experiments we tested the performance of a wide variety of ELM architectures and parameters, using both two-dimensional images one-dimensional vectors derived from these images.

Although CNNs are widely used for image classification, we found that, based on a substantial number of experiments, ELMs were able to outperform CNNs on the well-known Malimg dataset. The primary advantage of ELMs is faster training times as compared to CNNs. In our experiments, one CNN model typically required hours to train, while one ELM could be trained in a few seconds. This makes ELMs an option that should be considered for malware classification and detection, due to the large volume of new malware and variants released each year. ELMs have many detractors, but our experimental results strongly indicate that they can be competitive in the malware domain, at least in some situations.

For future work, it would be interesting to consider malware classification within broad types (trojan, worm, backdoor, etc.), rather than specific families. Experiments could also be conducted on other malware datasets and based on other techniques for converting executables to images. Our one-dimensional feature vector experiments suggest that for ELMs, it might not be necessary to consider images at all, and hence additional experiments with raw executable files would be worthwhile. Finally, many additional combinations of parameters could be considered, both for CNNs and ELMs.

## References

- [1] Anton Akusok, Kaj-Mikael Björk, Yoan Miché, and Amaury Lendasse. High-performance extreme learning machines: A complete toolbox for big data applications. *IEEE Access*, 3:1011–1025, 2015.

- [2] Jiuwen Cao, Jiaoping Hao, Xiaoping Lai, Chi-Man Vong, and Minxia Luo. Ensemble extreme learning machine and sparse representation classification. *Journal of the Franklin Institute*, 353(17):4526–4541, 2016.
- [3] Silvio Cesare and Yang Xiang. Classification of malware using structured control flow. In *Proceedings of the Eighth Australasian Symposium on Parallel and Distributed Computing - Volume 107*, AusPDC '10, pages 61–70, 2010.
- [4] François Chollet et al. Keras. <https://github.com/fchollet/keras>, 2015.
- [5] Extreme learning machine implementation in Python. <https://github.com/dclambert/Python-ELM>.
- [6] M. Farrokhmanesh and A. Hamzeh. A novel method for malware detection using audio signal processing techniques. In *2016 Artificial Intelligence and Robotics (IRANOPEN)*, pages 85–91, 2016.
- [7] Mehrdad Farrokhmanesh and Ali Hamzeh. Music classification as a new approach for malware detection. *Journal of Computer Virology and Hacking Techniques*, 15(2):77–96, Jun 2019.
- [8] Francisco Fernández-Navarro, César Hervás-Martínez, Javier Sanchez-Monedero, and Pedro Antonio Gutiérrez. MELM-GRBF: A modified version of the extreme learning machine for generalized radial basis function neural networks. *Neurocomputing*, 74(16):2502–2510, 2011.
- [9] Guang-Bin Huang, Qin-Yu Zhu, and Chee-Kheong Siew. Extreme learning machine: A new learning scheme of feedforward neural networks. In *2004 IEEE International Joint Conference on Neural Networks*, volume 2, pages 985–990, 2004.
- [10] Hashem Hashemi, Amin Azmoodeh, Ali Hamzeh, and Sattar Hashemi. Graph embedding as a new approach for unknown malware detection. *Journal of Computer Virology and Hacking Techniques*, 13(3):153–166, Aug 2017.
- [11] Gao Huang, Guang-Bin Huang, Shiji Song, and Keyou You. Trends in extreme learning machines: A review. *Neural Networks*, 61:32–48, 2015.
- [12] D. Hubel and T. Wiesel. Receptive fields, binocular interaction, and functional architecture in the cat’s visual cortex. *Journal of Physiology*, 160:106–154, 1962.
- [13] Amir Namavar Jahromi, Sattar Hashemi, Ali Dehghantanha, Kim-Kwang Raymond Choo, Hadis Karimipour, David Ellis Newton, and Reza M. Parizi. An improved two-hidden-layer extreme learning machine for malware hunting. *Computers and Security*, 89, 2019.
- [14] J. Zico Kolter and Marcus A. Maloof. Learning to detect and classify malicious executables in the wild. *Journal of Machine Learning Research*, 7:2721–2744, 2006.

- [15] Ashwini Majumdar, Gayatri Masiwal, and B. B. Meshram. Analysis of signature-based and behaviour-based anti-malware approaches. In *International Journal of Advanced Research in Computer Engineering and Technology*, volume 2, June 2013.
- [16] L. Nataraj, S. Karthikeyan, G. Jacob, and B. S. Manjunath. Malware images: Visualization and automatic classification. In *Proceedings of the 8th International Symposium on Visualization for Cyber Security, VizSec '11*, pages 4:1–4:7, New York, NY, USA, 2011. ACM.
- [17] M. Pak and S. Kim. A review of deep learning in image recognition. In *2017 4th International Conference on Computer Applications and Information Processing Technology*, pages 1–3, August 2017.
- [18] Igor Santos, Felix Brezo, Xabier Ugarte-Pedrero, and Pablo G. Bringas. Opcode sequences as representation of executables for data-mining-based unknown malware detection. *Information Sciences*, 231:64–82, 2013.
- [19] Igor Santos, Yoseba K. Penya, Jaime Devesa, and Pablo García Bringas. n-grams-based file signatures for malware detection. In *Proceedings of the 11th International Conference on Enterprise Information Systems, ICEIS 2009*, 2009.
- [20] Matthew G. Schultz, Eleazar Eskin, Erez Zadok, and Salvatore J. Stolfo. Data mining methods for detection of new malicious executables. In *Proceedings 2001 IEEE Symposium on Security and Privacy, SP '01*, pages 38–49, 2001.
- [21] Shahab Shamshirband and Anthony T. Chronopoulos. A new malware detection system using a high performance-elm method. In *Proceedings of the 23rd International Database Applications & Engineering Symposium, IDEAS '19*, pages 33:1–33:10, 2019.
- [22] Nitish Srivastava, Geoffrey Hinton, Alex Krizhevsky, Ilya Sutskever, and Ruslan Salakhutdinov. Dropout: A simple way to prevent neural networks from overfitting. *Journal of Machine Learning Research*, 15(1):1929–1958, 2014.
- [23] Mark Stamp. Deep thoughts on deep learning. <https://www.cs.sjsu.edu/~stamp/RUA/ann.pdf>, 2019.
- [24] Symantec. Internet security threat report. Technical report, Symantec, 2018.
- [25] Wing Wong and Mark Stamp. Hunting for metamorphic engines. *Journal in Computer Virology*, 2(3):211–229, 2006.
- [26] Ming Xu, Lingfei Wu, Shuhui Qi, Jian Xu, Haiping Zhang, Yizhi Ren, and Ning Zheng. A similarity metric method of obfuscated malware using function-call graph. *Journal of Computer Virology and Hacking Techniques*, 9(1):35–47, 2013.
- [27] Sravani Yajamanam, Vikash Raja Samuel Selvin, Fabio Di Troia, and Mark Stamp. Deep learning versus gist descriptors for image-based malware classification. In *Proceedings of the 4th International Conference on Information Systems Security and Privacy, ICISSP 2018*, pages 553–561, 2018.

- [28] Wei Zhang, Huan Ren, Qingshan Jiang, and Kai Zhang. Exploring feature extraction and ELM in malware detection for Android devices. In Xiaolin Hu, Yousheng Xia, Yunong Zhang, and Dongbin Zhao, editors, *Advances in Neural Networks*, ISNN 2015, pages 489–498, 2015.